Journal of Applied Fluid Mechanics, Vol. 17, No. 12, pp. 2514-2532, 2024.
Available online at www.jafmonline.net, ISSN 1735-3572, EISSN 1735-3645.
https://doi.org/10.47176/jafm.17.12.2770

Deep Learning-Based Eddy Viscosity Modeling for Improved RANS Simulations of Wind Pressures on Bluff Bodies

A. M. Aly†

Windstorm Impact, Science and Engineering (WISE) Research Lab, Louisiana State University, 3230 H Patrick F. Taylor Hall, Baton Rouge, LA 70803, USA

†*Corresponding Author Email: aly@LSU.edu*

ABSTRACT

Accurate prediction of wind pressures on buildings is crucial for designing safe and efficient structures. Existing computational methods, like Reynolds-averaged Navier-Stokes (RANS) simulations, often fail to predict pressures accurately in separation zones. This study proposes a novel deep-learning methodology to enhance the accuracy and performance of eddy viscosity modeling within RANS turbulence closures, particularly improving predictions for bluff body aerodynamics. A deep learning model, trained on large eddy simulation (LES) data for various bluff body geometries, including a flat-roof building and forward/backward facing steps, was used to adjust eddy viscosity in RANS equations. The results show that incorporating the machine learning-predicted eddy viscosity significantly improves agreement with LES results and experimental data, particularly in the separation bubble and shear layer. The deep learning model employed a neural network architecture with four hidden layers, 32 neurons, and tanh activation functions, trained using the Adam optimizer with a learning rate of 0.001. The training data consisted of LES simulations for forward/backward facing steps with width-to-height ratios ranging from 0.2 to 6. The study reveals that the machine learning model achieves a balance in eddy viscosity that delays flow reattachment, leading to more accurate pressure and velocity predictions than traditional turbulence closures like k-ω SST and k-ε. A sensitivity analysis demonstrated the pivotal role of eddy viscosity in governing flow separation, reattachment, and pressure distributions. Additionally, the investigation underscores the disparity in eddy viscosity values between RANS and LES models, highlighting the need for enhanced turbulence modeling. The findings presented in this paper offer substantive insights that can inform the advancement of more dependable computational methodologies tailored for engineering applications, encompassing wind load considerations for structural design and the intricate dynamics of unsteady aerodynamic phenomena.

Article History

Received April 8, 2024
Revised June 20, 2024
Accepted July 6, 2024
Available online October 2, 2024

Keywords:

Wind pressures
Deep learning
Eddy viscosity modeling
RANS simulations
Separation bubble
Shear layer
Bluff body aerodynamics

1. INTRODUCTION

1.1 Background

Wind engineering is crucial for ensuring the safety and stability of structures under environmental stressors like hurricanes and non-synoptic flows. Bluff body aerodynamics and wind structural engineering within the lower atmospheric boundary layer (ABL) involve complex phenomena that pose significant challenges in computational and experimental studies (Aly, 2014; Aly & Dragomirescu, 2018). The ABL is characterized by turbulence, velocity gradients, and Reynolds number effects, complicating the accurate prediction of wind effects on structures (Ai & Mak, 2015; Yan & Li, 2017; Liu & Stevens, 2020).

For decades, ABL wall-bounded wind tunnels have been used to investigate wind structural engineering issues and other environmental fluid mechanics problems. However, scale effects often limit their ability to accurately predict full-scale physics (Aly & Bitsuamlak, 2013; Aly, 2016; Aly et al., 2022). Computational fluid dynamics (CFD) has become popular for modeling wind effects, yet accurately predicting wind pressures on structures remains challenging. RANS simulations, in

particular, often fail to accurately predict wind pressures on bluff bodies, especially in the separation zone, such as flat roofs (Khaled & Aly, 2022). Although large eddy simulations (LES) are more accurate, they require significantly more time and resources.

Incorporating machine learning into CFD modeling may provide deeper insights into the shortcomings of RANS simulations in predicting wind-induced pressures in the shear layer (Aly & Gol-Zaroudi, 2020). Further research is necessary to enhance our understanding of bluff body aerodynamics and environmental fluid mechanics in the ABL (Ferreira et al., 2019; Gnatowska, 2019; San et al., 2019; Sharma et al., 2019; ElDegwy et al., 2022; Banari et al., 2023).

1.2 CFD Modeling

CFD modeling has gained popularity in wind engineering, aerodynamics, and fluid mechanics applications (TienPhuc et al., 2015; Ma & Lai, 2016; Zhang et al., 2017; Li et al., 2019; Dickison et al., 2020; Mahboub et al., 2022; Akhlaghi et al., 2023; Xingjun et al., 2023; Wadi Al-Fatlawi et al., 2024). However, accurately predicting wind pressures on structures remains challenging. RANS simulations are commonly employed but often yield inaccurate results due to turbulence closures rather than flow turbulence modeling. Although time-consuming and computationally expensive, LES simulations can be utilized to model wind effects. Resolving small spatiotemporal features incurs high computational costs, and there is a tradeoff between tractability and accuracy. An alternative approach involves employing a wall model for large-eddy simulation using the lattice Boltzmann method, which considers the wall's impact on the flow field and demonstrates its applicability to complex turbulent flows (Malaspinas & Sagaut, 2014).

However, in turbulent flows, the computational cost to resolve the small eddies increases by a factor proportional to the Reynolds number raised to the power of three. Therefore, if the Reynolds number is increased by a factor of 10, the computational cost is estimated to increase by a factor of 1000. This increase in computational expense makes LES challenging and DNS (direct numerical simulations) impractical for environmental fluid mechanics problems. Also, the same reason leads to the employment of RANS closures with LES on coarser grid arrangements, with a tradeoff of accuracy. A comparison between LES and wind tunnel experiments shows good agreement regarding mean velocity, turbulence statistics, and pressure distribution (Smolarkiewicz et al., 2007). The mesh generation, sizing, and convergence were explored for simulating atmospheric boundary layer flow to optimize the numerical simulation process (Gargallo-Peiró et al., 2018). Despite the increasing progress with LES, some limitations exist concerning the accuracy and computational requirements. The dependence of LES on the sub-grid scale (SGS) models is one of the main reasons for the inaccuracies (Kochkov et al., 2021). Simulating flow problems of higher Reynolds numbers creates challenges for CFD applications.

Turbulence modeling is essential for accurate and reliable CFD simulations, as turbulent flows are prevalent. Turbulence closures are required unless the expensive DNS is employed to directly solve the Navier-Stokes (NS) equations. The analysis of fluid motion, especially involving turbulence, is commonly achieved by applying NS equations. DNS is a technique that employs NS equations to resolve spatial and temporal turbulence numerically without any turbulence model (Orszag, 1970). This means that the turbulence's whole range of spatial and temporal scales must be resolved. DNS is currently deemed the most precise CFD method. However, it is restricted to low Reynolds number flows, as the computation cost increases substantially for higher Reynolds numbers. A flow model that combines the RANS equations and the continuity equation can be used to solve this issue. This simplified approach has proven to be a practical alternative to DNS (Zhou, 2017).

$$\frac{\partial \rho \mathbf{U}}{\partial t} + \nabla \cdot (\rho \mathbf{U}\mathbf{U}^T) = -\nabla p + \nabla \cdot (2\mu_m \mathbf{S} + \rho \mathbf{R}) + \rho f \quad (1)$$

$$\nabla \cdot \mathbf{U} = 0 \quad (2)$$

here, **U** is the fluid velocity vector, ρ is the density, **S** is a tensor representative of the mean strain rate, μm denotes the dynamic viscosity, p denotes pressure, **R** is a tensor containing the Reynolds stresses, and f is the externally applied force. The concept of molecular viscosity pertains to the transfer of momentum through molecular motion. In equation (1), the left-hand side comprises the temporal derivative of the convective acceleration and the local velocity, while the right-hand side accounts for the influence of external forces, pressure gradient, and viscosity. Per the Boussinesq assumption, the eddy viscosity is simulated by transferring momentum from turbulent eddies (Kundu et al., 2012). This approach draws upon the analogy between scalar transport and laminar momentum transport based on molecular motion and turbulent momentum transport and scalar transport based on eddy motion, as explained by Kundu et al. (2012). In the context of the RANS closure, the parameter R is defined as follows.

$$\mathbf{R} = -\overline{u' u'^T} = 2\frac{\mu_t}{\rho}\mathbf{S} - \frac{2}{3}k\delta_{ij} \quad (3)$$

$$\mathbf{S} = \frac{1}{2}(\nabla \mathbf{U} + (\nabla \mathbf{U})^T) \quad (4)$$

in which k is the kinetic energy of turbulence, μt denotes eddy viscosity, u' represents the velocity fluctuating component, and δij refers to the Kronecker delta. Reynolds stresses emerge due to the advection term in the momentum conservation equation, which embodies the mean stresses of fluctuations (Kundu et al., 2012). Reynolds stresses can be regarded as the pace of transfer of mean momentum that results from the fluctuations in the flow and are generally more substantial than the viscous stresses, except in the proximity of a solid surface where the fluctuations become negligible.

The Reynolds stress terms are not readily known and necessitate a turbulence closure to solve the RANS equations. Turbulence closures can be categorized using additional equations to approximate the Reynolds stress terms. They can vary from simplistic algebraic

expressions to highly intricate relations that exhibit high fidelity. In RANS simulations, the two-equation models are predominantly employed. Turbulence closures typically consist of equations for turbulence kinetic energy and turbulent length scale (Menter, 1992). The most commonly used turbulence closures in RANS simulations are the k-ε and k-ω closures. The k-ε closure was initially developed in 1973 and has undergone several refinements since (Jones & Launder, 1973). The eddy viscosity, μt, is expressed as follows:

$$\mu_t = C_\mu \rho \frac{k^2}{\varepsilon} \tag{5}$$

where k refers to the turbulence kinetic energy, ε denotes the dissipation rate, and Cμ is a constant (Aly & Dougherty, 2021). Turbulence closures for RANS simulations exhibit limitations due to their underlying assumptions. One way to address this is to use models like LES to resolve most turbulence energy and only approximate the sub-grid portion. Recently, machine learning has gained significant attention as a tool for accelerating the solution of complex flow problems in various applications. In CFD, machine learning can be used for shape optimization studies and predicting results for untested cases based on high-fidelity simulations.

The choice of SGS models with LES and hybrid RANS-LES models significantly influences CFD simulations' computational time and accuracy. The author investigated the effects of different SGS models on empty-domain flow features and found that LES (with WALE SGS model) and DES offer higher accuracy than other widely used SGS versions (Khaled et al., 2021). Wall-modeled LES and hybrid RANS-LES offer more realistic solutions to identified issues (Slotnick et al., 2014).

Applying deep learning in CFD can reduce computational costs and increase accuracy significantly (Zan et al., 2022; Bao et al., 2023; Chen et al., 2023). Recent empirical research has demonstrated that leveraging machine learning techniques can significantly expedite computational fluid dynamics simulations while maintaining high fidelity and precision in the computed results (Zhao et al., 2021; Zhu et al., 2022). Hybrid ML-PDE techniques and artificial neural network models can be instrumental in turbulent flow simulations and wake prediction of wind turbines (Pathak et al., 2020).

1.3 Machine Learning and Computational Fluid Dynamics

Machine learning (ML) has emerged as a promising approach for enhancing the precision and efficiency of CFD simulations (Singh et al., 2017; Pathak et al., 2020; Ti et al., 2020; Kochkov et al., 2021). Recent studies have demonstrated the potential of ML-enabled CFD simulations to yield more accurate outcomes than conventional RANS closures (Duraisamy et al., 2019; Zhao et al., 2020).

Moreover, ML-based approaches have shown promising results in improving the accuracy and efficiency of RANS turbulence closures. Researchers have proposed innovative ML-based methods, such as convolutional neural networks (CNNs), iterative ML frameworks, and Bayesian deep neural network (BDNN) approaches, to address challenges in RANS modeling (Fukami et al., 2019; Geneva & Zabaras, 2019; Liu et al., 2021). These approaches have been shown to outperform traditional RANS closures, especially for complex flow scenarios.

In recent studies, novel materials such as black phosphorus (BP) have shown promise in controlling fluid transmission devices due to their unique surface properties (Zhang et al., 2019). Additionally, innovative fluid dynamics models, such as the 'channel moving' pressure-driven model, have been proposed to generate constant pressure gradients in fluid flow, offering insights into atomistic-to-continuum coupling and the applicability of classical fluid dynamics equations in nanochannel flow width. These advancements highlight the potential of integrating novel materials and fluid dynamics models to enhance membrane technology and fluid transmission systems.

Majchrzak et al. (2023) reviewed the challenges associated with traditional numerical methods for simulating turbulent flows and explored how machine learning approaches, including closure models, direct modeling, and hybrid modeling, can potentially overcome some of these challenges (Majchrzak et al., 2023). The review concludes that ML has the potential to improve the accuracy and efficiency of turbulent flow simulations significantly but requires further research to understand its capabilities and limitations fully. In this paper, machine learning is used to manipulate the eddy viscosity in RANS simulations for improved prediction of wind pressures on bluff bodies. While ML techniques hold significant potential for advancing RANS modeling in CFD, further research is needed to understand their capabilities and limitations fully. Continued exploration of ML-based approaches in turbulent flow simulations could lead to more accurate and efficient CFD simulations in various applications.

1.4 Novelty and Originality

Despite significant advancements in wind engineering and CFD, accurately predicting wind pressures on bluff bodies using RANS simulations remains challenging. Current computational approaches struggle with turbulence closures that inadequately model complex flow phenomena in separation zones and shear layers. This research addresses this gap by integrating machine learning with CFD to enhance the precision and efficiency of RANS simulations. We train a deep learning model on LES data to manipulate eddy viscosity in RANS closures, improving the capture of flow physics in critical areas. This novel methodology provides more accurate predictions of wind pressures on bluff bodies and enhances the reliability of computational approaches in wind engineering and environmental fluid mechanics. Furthermore, the proposed approach offers valuable insights into the role of eddy viscosity in understanding the fundamental aerodynamics of separation zones and shear layers, contributing to a deeper comprehension of the underlying flow dynamics.

1.5 Objectives and Paper Layout

Environmental fluid mechanics studies in CFD are challenging due to limitations in current turbulence models, which struggle with accurately predicting complex flow behavior. These models face issues related to accuracy, stability, and efficiency. Deep learning offers promising improvements in these areas, potentially yielding more accurate results than traditional RANS simulations. This paper aims to investigate the accuracy of RANS simulations in predicting wind effects on flat roofs, particularly in the presence of flow separation. We focus on two main hypotheses: (1) inaccurate RANS simulations are due to flawed eddy viscosity closure approximations, and (2) machine learning can effectively train models to produce eddy viscosity for RANS equations. We detail the simulation setup and machine learning-based eddy viscosity modeling methodology to test these hypotheses. We then present and analyze the results, comparing the accuracy of machine learning-based RANS simulations with conventional RANS and LES results. Additionally, we examine the role of eddy viscosity in RANS simulation accuracy and roof pressure predictions in flow separation contexts. The paper is structured clearly and logically, guiding the reader through the research process. Section 2 provides a comprehensive overview of the research methodology, ensuring transparency and replicability. Section 3 presents the study's results, highlighting the key findings and their significance. The discussion in Section 4 delves deeper into the implications of these results, drawing connections to existing literature and exploring potential applications. Finally, Section 5 concisely summarizes the main conclusions drawn from the research, emphasizing the importance of the study and its contributions to the field.

2. METHODOLOGY

The aerodynamic characteristics of bluff bodies, such as low-rise buildings situated in the atmospheric boundary layer (ABL), are governed by complex flow phenomena, including flow separation, reattachment, vortex shedding, and other unsteady features. An accurate representation of these complex flow features is crucial for predicting wind-induced pressures on flat roofs (Khaled & Aly, 2023). The effectiveness of ML-based RANS simulations is investigated for flat roofs by conducting simulations on a full-scale cube in the 'open country' at Silsoe, UK. This location has been previously subjected to extensive measurement and analysis of surface pressures along the vertical ring of the Silsoe cube (Richards & Hoxey, 2002, 2012). The Silsoe cube is a field experimental building designed for wind pressure measurements. It is a 6 m x 6 m x 6 m cube-shaped building with a flat roof and four identical sides. The building was constructed in the early 1990s by the Building Research Establishment (BRE) at their Silsoe Research Institute site in Bedfordshire, UK. The purpose of the Silsoe cube was to study the wind pressures on a simple cube-shaped building to improve building design standards for wind loading. The Silsoe cube has since been used extensively in wind engineering research and has become a widely recognized benchmark for evaluating CFD models of wind pressure on buildings. Integrating the ML model with the OpenFOAM software aims to enhance RANS simulations' precision and computational efficiency. The ML model accurately estimates the eddy viscosity in RANS simulations and enables faster and more accurate simulations (Maulik et al., 2021). The results are then compared with those from LES, commonly used in building aerodynamics due to the limitations of RANS closures in predicting complex phenomena such as flow separation.

To investigate the accuracy of the ML-based RANS simulations, we introduced a forward/backward step geometry into the computational domain, as illustrated in Fig. 1. The grid independence study is a crucial step in ensuring the accuracy and reliability of CFD simulations. To assess the influence of mesh resolution on the results, three different grids were employed: a low-resolution grid with 670,992 cells, a medium-resolution grid with 738,624 cells, and a high-resolution grid with 2,525,196 cells.

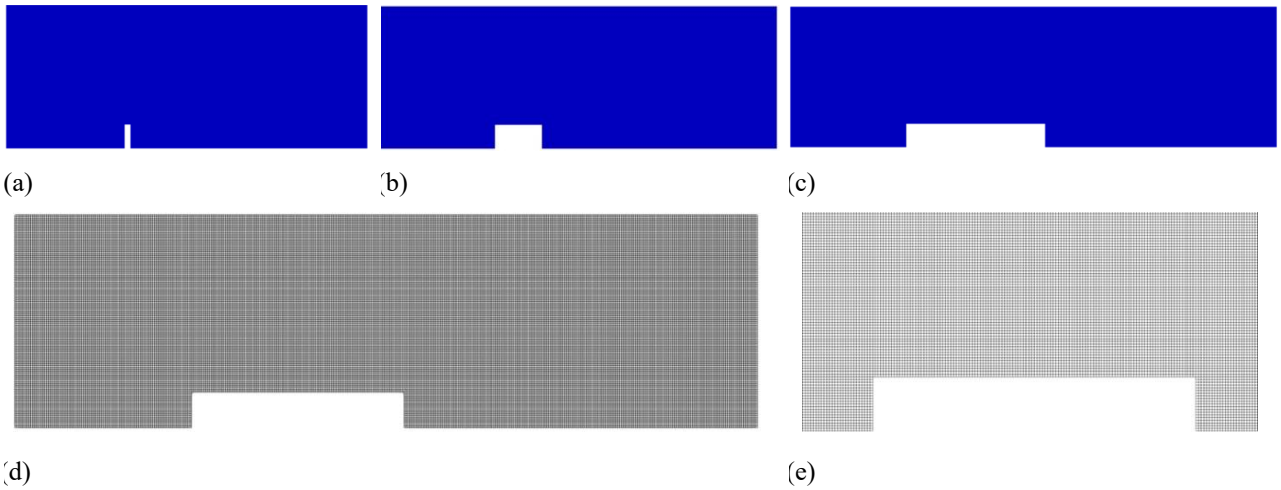

Fig. 1 Sample geometries of forward/backward facing steps used for training the deep learning model. (a-c) Variations in step width (w) relative to step height (h): (a) w = 0.2h, (b) w = 2h, and (c) w = 6h. (d) High-fidelity prismatic mesh generated for w = 6h case. (e) Magnified view of the mesh near the step

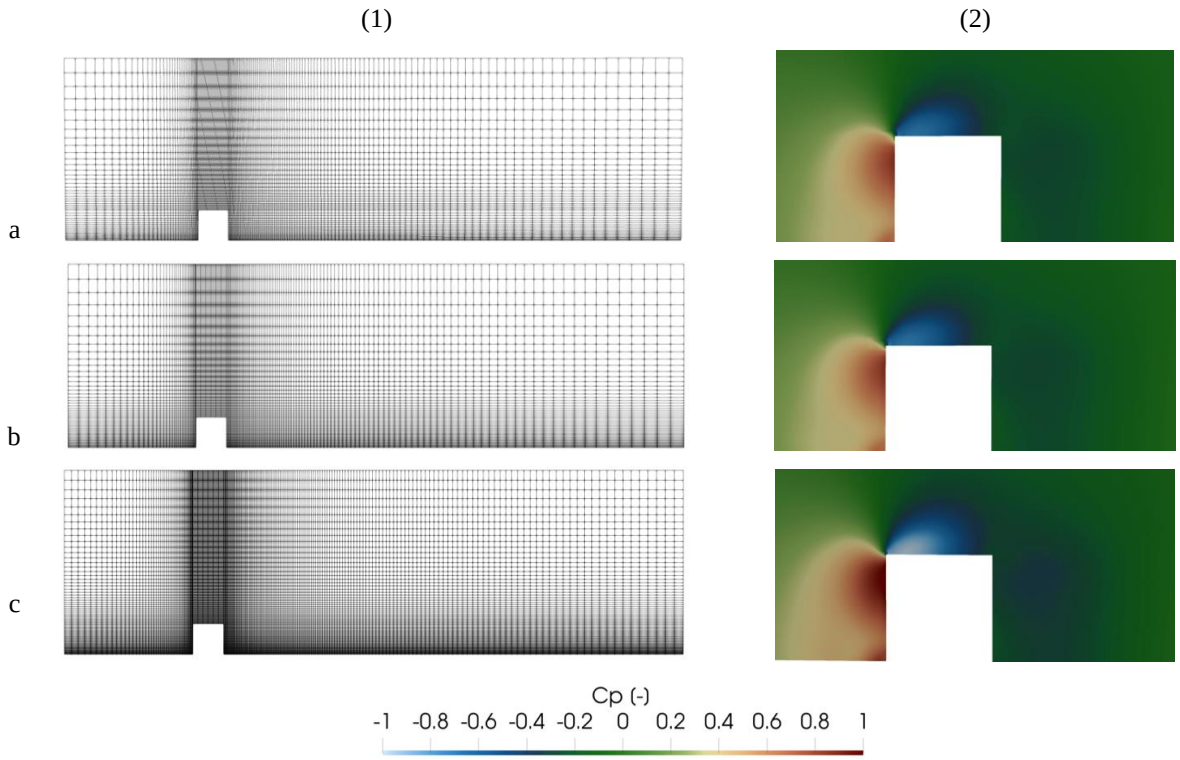

Fig. 2 Grid independence study for pressure coefficient predictions using the k-ω SST turbulence closure. (a1) Low-resolution mesh with 670,992 cells. (a2) Pressure coefficient distribution on the low-resolution mesh. (b1) Medium-resolution mesh with 738,624 cells. (b2) Pressure coefficient distribution on the medium-resolution mesh. (c1) High-resolution mesh with 2,525,196 cells. (c2) Pressure coefficient distribution on the high-resolution mesh. Results demonstrate grid convergence of the pressure predictions as the mesh is refined

Figure 2 illustrates the mesh characteristics and corresponding pressure coefficient distributions for each grid level, obtained using the k-ω SST turbulence closure. The low-resolution grid (Fig. 2a(1)) exhibits a relatively non-uniform cell size, while the medium-resolution grid (Fig. 2b(1)) incorporates localized refinement around the cube to capture flow details more accurately. The high-resolution grid (Fig. 2c(1)) further enhances the resolution, particularly in the near-wall regions, to better resolve boundary layer effects. The pressure coefficient distributions (Fig. 2, column (2)) demonstrate the impact of grid resolution, with the finer meshes capturing more intricate flow features and pressure variations around the cube. A time step of 0.001 s was used for LES simulations to maintain a Courant number of less than 1.

LES were conducted for several cases with width-to-height (w/h) ratios of 0.2, 0.5, 0.75, 1, 1.25, 1.75, 2, 3, 4, and 6. High-quality prismatic element meshes were generated using the OpenFOAM blockMesh utility. Figure 3 displays a sample of the LES results utilized for the ML model training. The contours represent the instantaneous velocity and averaged total turbulent kinetic energy for different w/h ratios, which were employed to calculate the eddy viscosity. The data from LES simulations, including the velocity, eddy viscosity, and depth of the forward/backward-facing step, are used later to train the ML model to predict eddy viscosity for a given velocity and depth.

Recently, researchers have actively explored integrating machine learning (ML) techniques to reduce the computational burden associated with CFD simulations. The term "machine learning" was coined by Arthur Samuel, a pioneering computer scientist at IBM, in 1959 (Samuel, 1959, 1962). ML encompasses a broad range of methods that leverage data to enhance the performance of various tasks (Mitchell, 1997). The primary categories of ML algorithms include supervised, unsupervised, and reinforcement learning approaches. Supervised learning algorithms map labeled input data to known output targets, typically addressing regression and classification problems. On the other hand, unsupervised learning techniques aim to uncover underlying patterns and structures within datasets, facilitating dimensionality reduction and clustering tasks. Reinforcement learning algorithms learn through a trial-and-error process, iteratively refining their decision-making strategies to solve control problems.

At the core of ML lies the optimization of model parameters based on available data. Neural networks, a prominent class of ML models, are designed to mimic the information-processing capabilities of the human brain. In its most fundamental configuration, neural network architectures are composed of input layers, hidden layers, and output layers, as illustrated in Fig. 4. The input neurons receive and classify the input information, which is subsequently transmitted through the intervening neural network layers until arriving at the output layer, where the ultimate inference is generated.

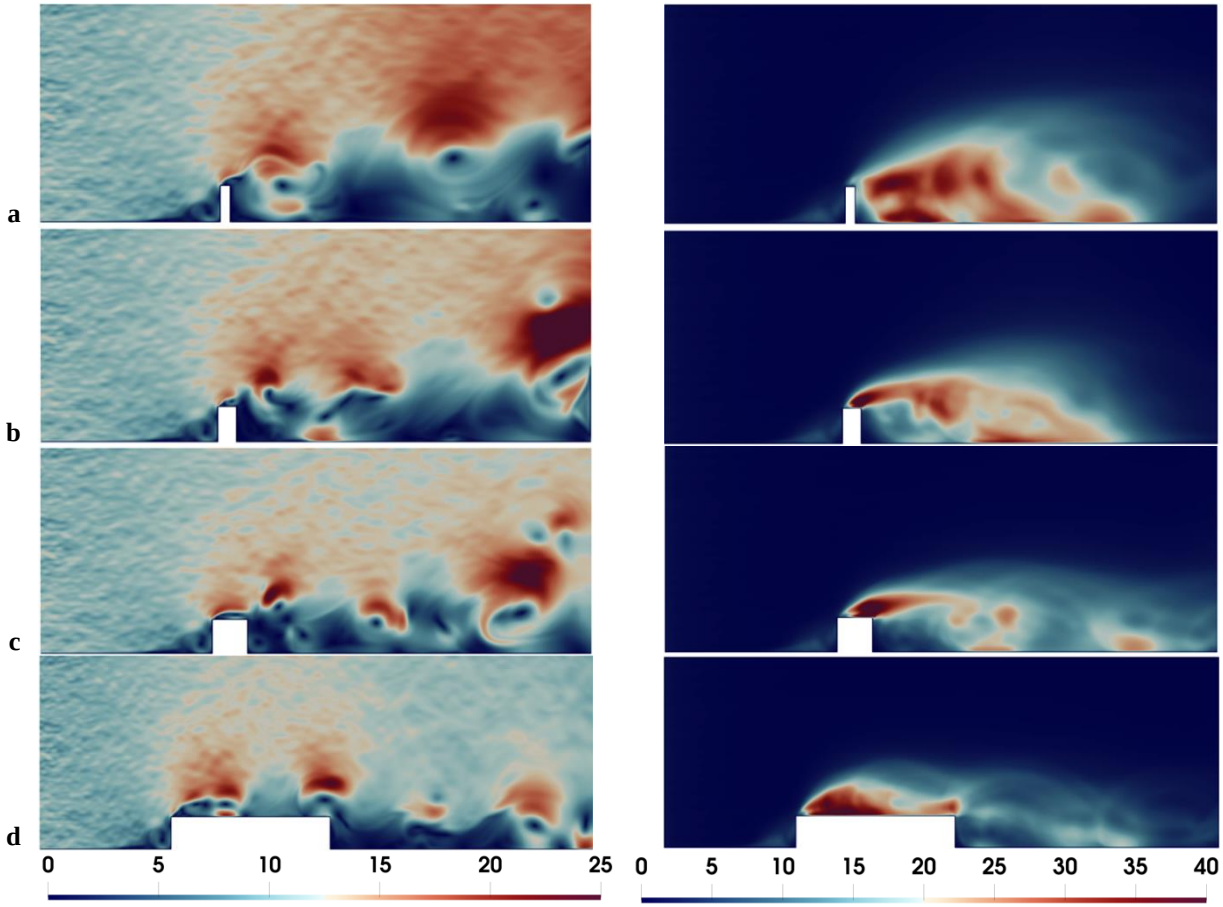

Fig. 3 Sample LES results for forward/backward facing steps with varying width-to-height ratios (w/h). Column 1 shows contours of instantaneous velocity (m/s), while Column 2 depicts contours of averaged total turbulent kinetic energy (m^2/s^2) for step geometries with (a) w = 0.2h, (b) w = 0.5h, (c) w = h, and (d) w = 6h. The LES data were used as training inputs for the deep learning model to predict eddy viscosity for a given step geometry

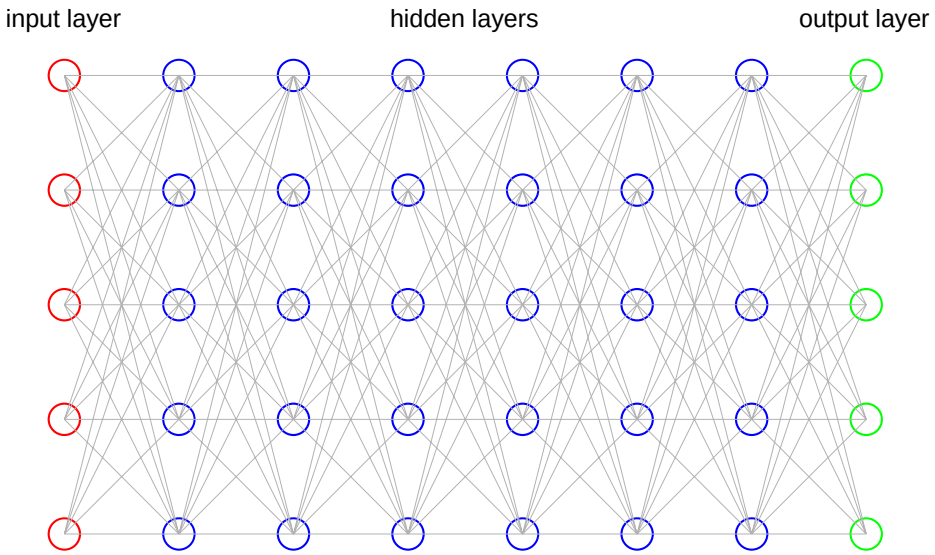

Fig. 4 Schematic of a typical feedforward neural network architecture. The network consists of an input layer that receives the input data, one or more hidden layers that apply transformations to the data, and an output layer that produces the final predictions. Each layer is composed of interconnected nodes or neurons. The connections between neurons have associated weights that are adjusted during training to optimize the network's performance. The data propagates unidirectionally from the input to the output layer without recurrent connections or feedback mechanisms

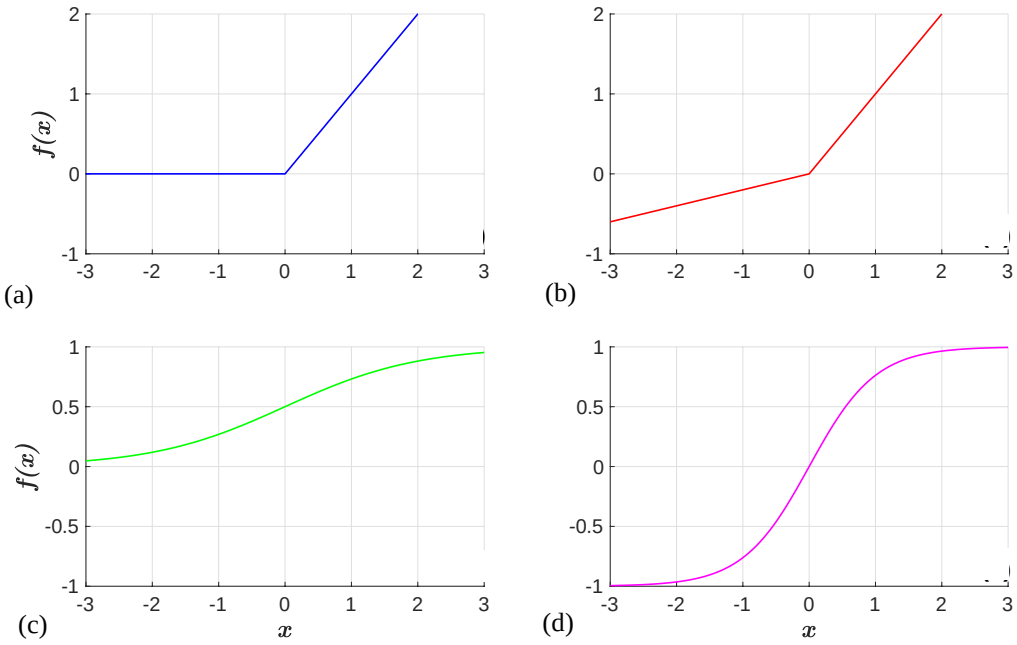

Fig. 5 Common activation functions used in neural networks: (a) ReLU: outputs x if positive, 0 otherwise. Simple yet effective. (b) Leaky ReLU: similar to ReLU but assigns a slight positive slope to negative values. (c) Sigmoid: squashes any input to range (0, 1). Useful for modeling probabilities. (d) Tanh: outputs values in the range (-1, 1). Zero-centered can be advantageous over sigmoid. The current study employed tanh activation for input and hidden neural network layers. The choice of activation function depends on the specific problem and architecture

Each neuron in a neural network is assigned a weight and a threshold value, with the weight matrices represented by the connections between neurons in the network diagram. The weighted sum of the inputs at each node in an artificial neural network is passed through an activation function. Based on a predefined activation threshold, this function determines whether the node's output value will be propagated to the next layer. The incorporation of an activation function within the neural network architecture serves to introduce nonlinear properties. This enables the model to effectively learn and capture intricate relationships inherent in the input data, facilitating the approximation of complex functions.

Several parameters play a crucial role in evaluating and performing neural network models. One essential parameter is the choice of activation functions applied to the weighted sum at each neuron. Neural networks model complex functions by constructing networks of interconnected nodes (Fig. 5). These nodes accumulate values from previous nodes through an activation function g. For a layer l in the network, the output of the i^{th} node $a_{i,l}$ is computed as follows (Thuerey et al., 2020; Aly & Clarke, 2023):

$$a_{i,l} = g\left(\sum_{j=0}^{n_{l-1}} w_{ij,l-1}\, a_{j,l-1}\right) \quad (6)$$

where n_{l-1} is the total number of nodes in layer l-1, and w is the weight.

The rectified linear activation function (ReLU) provides an output if its input is positive. Otherwise, the output is zero (Fig. 5-a). The leaky ReLU is a type of ReLU that defines a slight slope that leaks some positive values to zero if they are close enough to zero (Fig. 5-b). Other activation functions include the sigmoid and tanh functions (Fig. 5-c&d). The tanh activation function was employed for both input and hidden layers during training, as it provided better performance than the other options. A learning rate of 0.001 was used for the optimization.

Deep learning using TensorFlow in OpenFOAM was implemented to accelerate fluid flow simulations. The methodology was based on the steps outlined by Maulik et al. (2021). TensorFlow was integrated with OpenFOAM by installing the TensorFlow library and configuring the OpenFOAM environment to recognize TensorFlow (Maulik et al., 2021). A TensorFlow neural network model was created and trained using data from LES simulations on the forward/backward step. The neural network was designed to predict fluid flow outcomes based on inputs such as flow conditions, boundary conditions, and geometry. The calculated results of the eddy viscosity, velocity, and coordinates from 10 LES simulations were used to train the ML model. The training dataset consisted of eight samples; the remaining two were used for testing. The predicted eddy viscosity for a given step width is obtained as the output of the ML model, which consists of four hidden layers and 32 neurons. The eddy ML-obtained eddy viscosity was then used to solve the RANS equations.

The training results are depicted in Fig. 6. The model was validated by comparing its predictions with actual LES OpenFOAM simulation results and experimental data from the literature. The trained neural network model was used to manipulate the eddy viscosity to understand its role in the flow properties such as velocity and pressure.

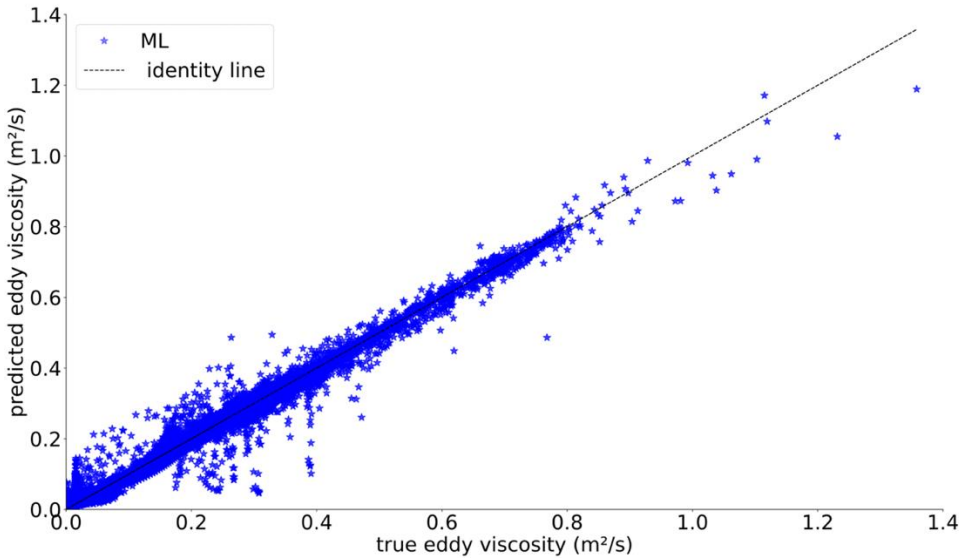

Fig. 6 Comparison of machine learning predicted eddy viscosity (m²/s) versus the ground truth values from LES data. The neural network was trained on LES results for forward/backward facing steps with varying width-to-height ratios. The close agreement between the ML predictions and LES data demonstrates the ability of the trained model to accurately estimate the eddy viscosity field for flow around bluff bodies

3. RESULTS

The results from various RANS simulation cases are analyzed to obtain the distribution of the mean C_p along the vertical ring, and these are compared with reference LES results. It is well known that RANS turbulence closures often fail to predict complex flow scenarios such as flow separation accurately. Our findings align with this observation; all RANS cases fail to reproduce the magnitude and pattern of the mean C_p in the flow-separated zone, particularly on the roof. The k-ε turbulence closure's limitations prompted using the k-ω SST closure, but the two closures did not accurately recreate the flow physics in the flow-separated zone.

Figure 7 shows that the pressure coefficient obtained by the ML approach is close to the LES and experimental results from the literature (Lim et al., 2007; Guichard, 2019). The ML model outperforms the k-ε and k-ω SST turbulence closures in predicting mean pressures on the roof, especially in the flow-separated zone. The k-ε closure produced higher negative pressures near the windward side but significantly lower negative pressure on the rest of the roof, explained further by the velocity contour in Fig. 8).

As shown in Fig. 8a, the flow reattaches to the roof in the k-ε case, resulting in less suction, except near the windward side, where the magnitude of negative pressure is significantly high. The k-ω closure experiences significant flow separation on the roof, with a more uniform pressure distribution (Fig. 8b), leading to uniform negative pressure on the roof (Fig. 7). The ML model shows flow separation at the windward side, with minor reattachment near the leeward side (Fig. 8c), consistent with pressures in Fig. 7.

The eddy viscosity was studied to understand the flow physics and the discrepancies between LES and RANS simulations on the Silsoe cube further. Using a Notebook PC with 12 cores and 40 GB of available memory, the k-ε turbulence closure took about 21.75 minutes to converge, the k-ω SST took 44.3 minutes, the ML took 6.27 minutes, and the LES took about 5.6 hours.

Figure 9 displays the eddy viscosity contour maps for the RANS and ML simulations. The eddy viscosity values predicted by the k-ε, k-ω SST, and LES-based ML model differed significantly. The ML model produced higher eddy viscosity values on the roof and in the wake of the bluff body (ranging between 0.05 and 0.5 m²/s). In comparison, the RANS closures produced lower and more uniform eddy viscosity values on the roof and wake of the cube (0.2 m²/s). However, the RANS simulations predicted higher eddy viscosity values towards the upper boundary than the ML model. These differences highlight the importance of eddy viscosity as a critical parameter in generating roof pressure.

To investigate the sensitivity of roof pressure to eddy viscosity, we systematically varied the eddy viscosity values in the ML model by multiplying them by a factor ranging from 0.2 to 10, where 1 signifies the original LES-produced eddy viscosity, 0.2 denotes smaller values, and 10 indicates values ten times larger.

Figure 10 illustrates the impact of varying eddy viscosity on the velocity contours around the bluff body. The contours reveal that increasing the eddy viscosity leads to a higher degree of flow reattachment on the leeward side of the bluff body, as evidenced by the backward movement of the reattachment point. This leads to significantly less negative pressure on most of the leeward surface but higher negative pressures near the windward side, as shown in Fig. 7 (k-ε results). This is consistent with the velocity and eddy viscosity contours for the k-ε RANS model shown in Fig. 8a and Fig. 9a, respectively. The k-ε model predicts higher eddy viscosity

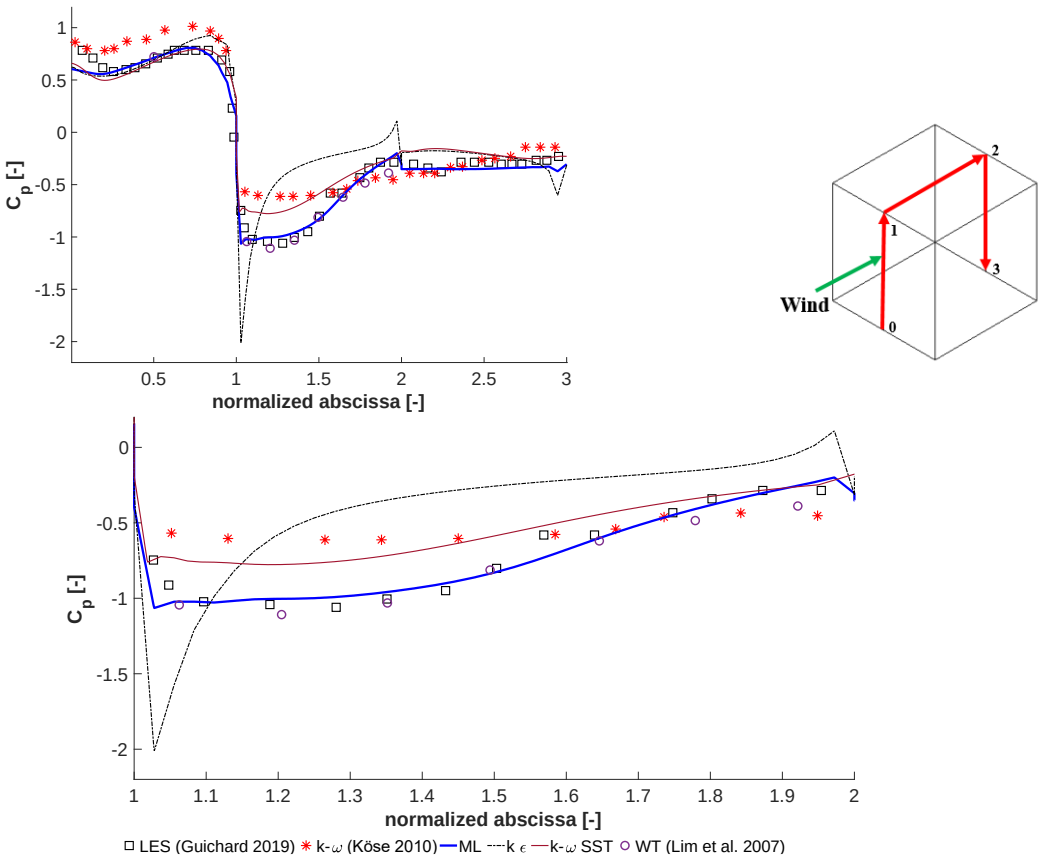

Fig. 7 Comparison of roof pressure coefficients (Cp) obtained from ML, LES, RANS simulations using k-ε and k-ω SST turbulence closures, and experimental data. The ML approach closely matches the LES results and experimental data, particularly in the flow separation region on the roof. In contrast, the k-ε model predicts higher negative pressures near the windward roof edge due to a small, tight separation bubble, while the k-ω SST model underpredicts the negative pressures on most of the roof. The ML model's ability to accurately capture the pressure distribution, especially in the separated flow region, demonstrates its effectiveness in improving RANS simulations of bluff body aerodynamics compared to traditional turbulence closures

values in the separation region compared to the machine learning approach, resulting in a small separation bubble near the windward side of the roof (with a sharp increase in the negative pressure) and early reattachment that reduced the magnitude of the negative pressure on most of the roof towards the leeward side.

In contrast, decreasing the eddy viscosity in the ML model resulted in the reattachment point moving forward, leading to more negative pressure on most of the leeward surface but still high negative pressures near the windward side, as shown in Fig. 7 (k-ω SST results). This is consistent with the velocity and eddy viscosity contours for the k-ω SST RANS model shown in Fig. 8b and Fig. 9b, respectively. The k-ω SST model predicts lower eddy viscosity values in the separation region than the machine learning approach, resulting in a more significant separation bubble and delayed reattachment.

These results further demonstrate the pivotal role of eddy viscosity in governing the flow separation, reattachment, and pressure distribution around bluff bodies, which is accurately captured by the machine learning enhanced RANS approach. The k-ε model's higher eddy viscosity in the separation region leads to faster reattachment and reduced negative pressures on the leeward side, while the k-ω SST model's lower eddy viscosity results in delayed reattachment and larger separation bubbles. The machine learning approach strikes a balance in eddy viscosity prediction, leading to a more accurate representation of the flow physics compared to traditional RANS turbulence closures.

4. DISCUSSION OF RESULTS

In this study, machine learning (ML) models were trained to manipulate eddy viscosity in Reynolds-averaged Navier-Stokes (RANS) simulations, improving accuracy in predicting fluid dynamics phenomena. The research aimed to identify the fundamental elements responsible for the variances between forecasted and observed mean pressure values in RANS (Reynolds-Averaged Navier-Stokes) simulations when assessing the influence of wind on flat roof structures. The results confirm these inaccuracies stem from limitations in the eddy viscosity closure approximation used in RANS turbulence models. LES data was used to train an ML model that provides accurate eddy viscosity for RANS simulations to address this. The Silsoe cube, including forward- and backward-facing steps, was modeled to train the machine learning model for CFD RANS simulations.

The findings indicate that the eddy viscosity provided

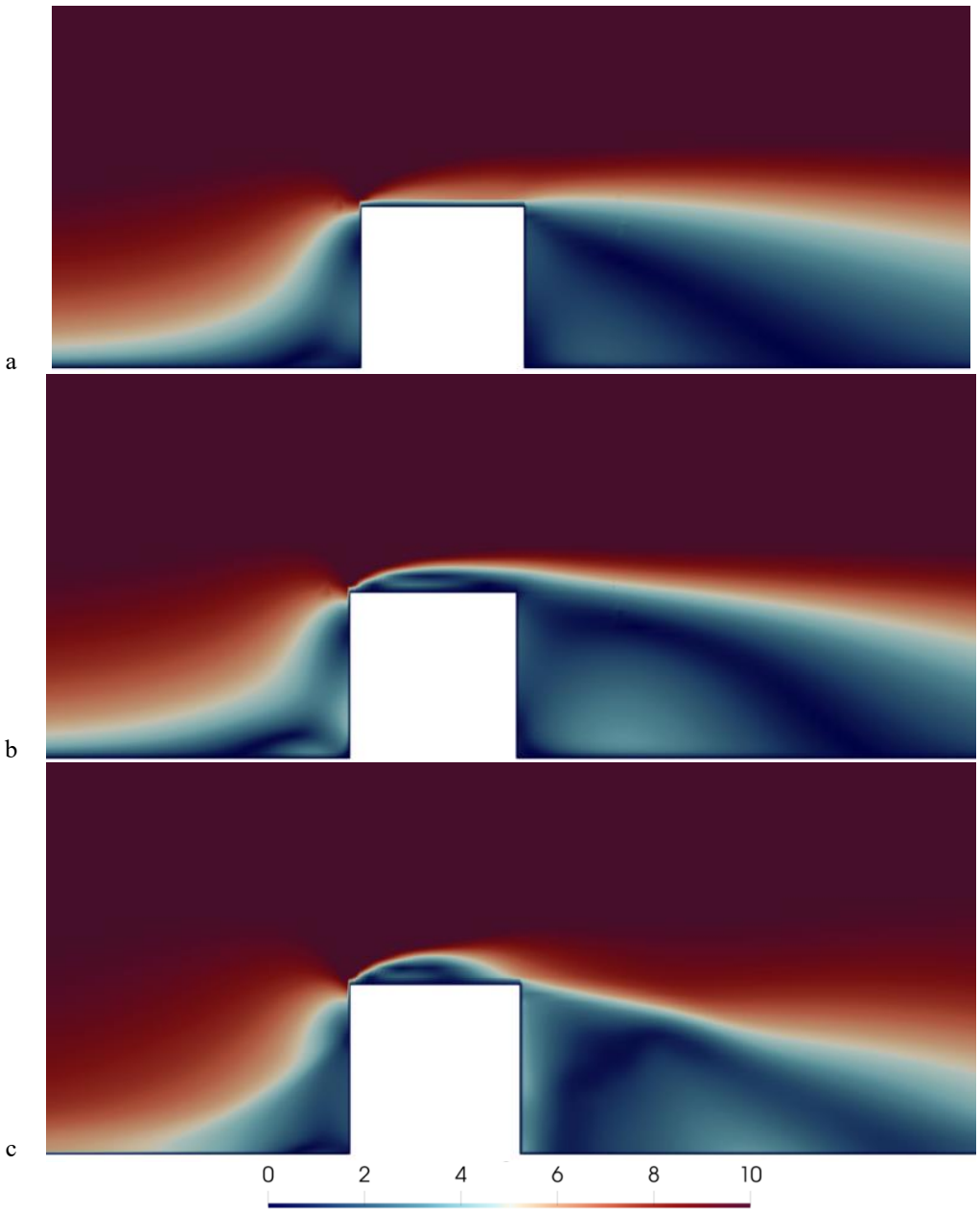

Fig. 8 Velocity contours from ML and RANS simulations (m/s): (a) k-ε, (b) k-ω SST, and (c) ML. Comparison of velocity contours (m/s) around the bluff body obtained from (a) k-ε RANS, (b) k-ω SST RANS, and (c) machine learning (ML) enhanced RANS simulations. The ML approach closely matches the velocity field predicted by high-fidelity LES, particularly in the flow separation region on the leeward side of the bluff body. In contrast, the k-ε model shows faster flow reattachment, while the k-ω SST model predicts a larger separation bubble. The ML model's ability to accurately capture the velocity distribution, especially in the separated flow region, demonstrates its effectiveness in improving RANS simulations of bluff body aerodynamics compared to traditional linear eddy-viscosity turbulence models

by the ML model differs significantly from that predicted by the k-ε and k-ω SST closures. However, the pressures predicted by the ML-based eddy viscosity align more closely with those from LES simulations.

To further understand why RANS simulations fail to predict roof pressures accurately, the performance of the LES model was compared against two conventional RANS closures (k-ε and k-ω SST) in predicting the flow field in the standard PitzDaily problem (Le et al., 1997). The two RANS closures incorrectly predict the eddy viscosity (Fig. 11), leading to incorrect velocity (Fig. 12) and pressure contours Fig. 13).

Both conventional RANS closures failed to accurately predict the eddy viscosity compared to the LES reference data (Fig. 11). These inaccuracies lead to significant discrepancies in the velocity and pressure contours (Fig. 12 and Fig. 13). Conversely, the ML model's eddy viscosity predictions agree well with LES data, resulting

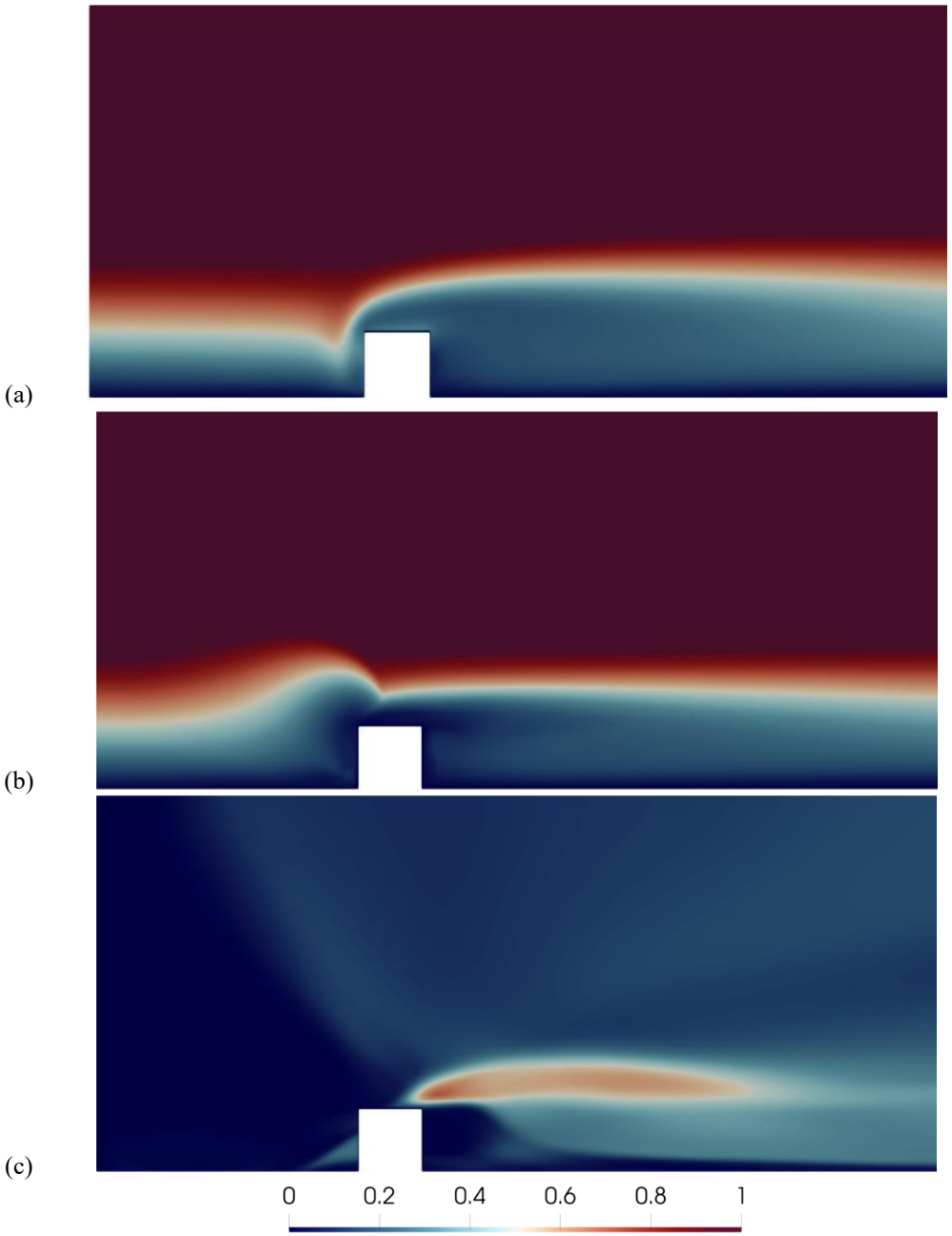

Fig. 9 Comparison of eddy viscosity contours (m^2/s) obtained from (a) k-ε RANS, (b) k-ω SST RANS, and (c) machine learning (ML) enhanced RANS simulations. The ML approach predicts higher eddy viscosity values near the leeward side of the bluff body, particularly in the flow separation region and wake. In contrast, the k-ε and k-ω SST models show lower eddy viscosity in this area. Conversely, the RANS closures exhibit higher eddy viscosity near the upper boundary of the computational domain. The balanced distribution of eddy viscosity predicted by the ML model, both in magnitude and spatial distribution, leads to a more accurate flow physics representation than traditional linear eddy-viscosity turbulence models

in improved velocity and pressure predictions. These findings support the hypothesis that the failure of RANS simulations to predict roof pressures is due to the inaccurate modeling of eddy viscosity in the separation bubble and shear layer.

Notably, the LES results used in this study are considered more accurate than RANS predictions, as they are closer to DNS counterparts (Le et al., 1997). However, LES is computationally expensive and may not be feasible for practical engineering applications. The research presented herein investigates the efficacy of machine learning methodologies in expediting and enhancing RANS simulations, thereby facilitating precise forecasts of wind-induced pressures acting upon planar roof surfaces.

The incorrect representation of eddy viscosity has significant implications for the accuracy of mean pressure predictions and, consequently, the reliability of RANS simulations. Specifically, the findings reveal the limitations of RANS simulations in predicting roof pressures, primarily due to the inability to predict eddy viscosity effectively in the separation bubble and shear layer.

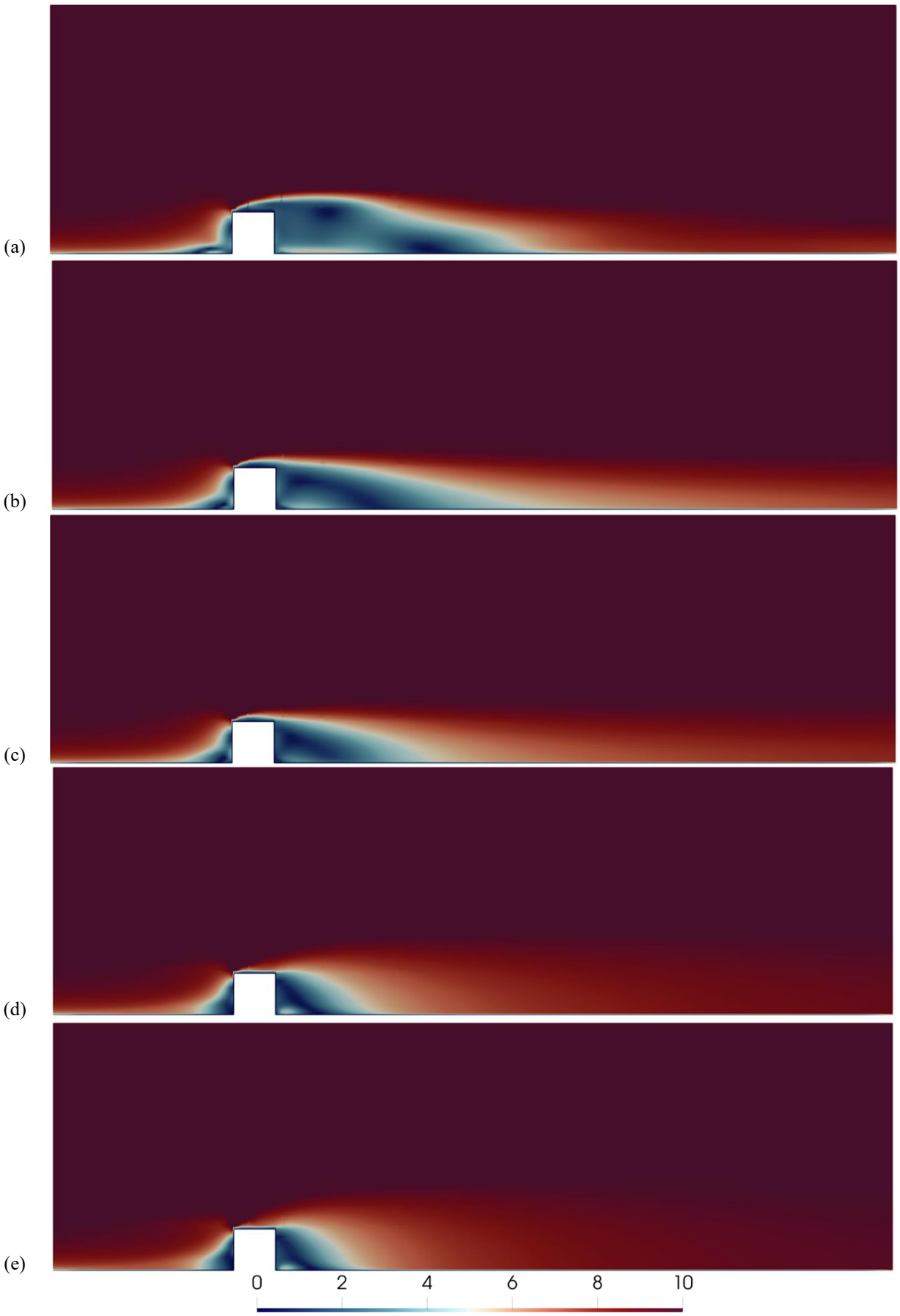

Fig. 10 Effect of varying eddy viscosity on the flow velocity (m/s) around the bluff body. Velocity contours are shown for eddy viscosity values of (a) 0.2, (b) 0.6, (c) 1 (nominal), (d) 5, and (e) 10 times the eddy viscosity predicted by the ML model. Increasing the eddy viscosity leads to a higher degree of flow reattachment on the leeward side of the bluff body, as evidenced by the backward movement of the reattachment point

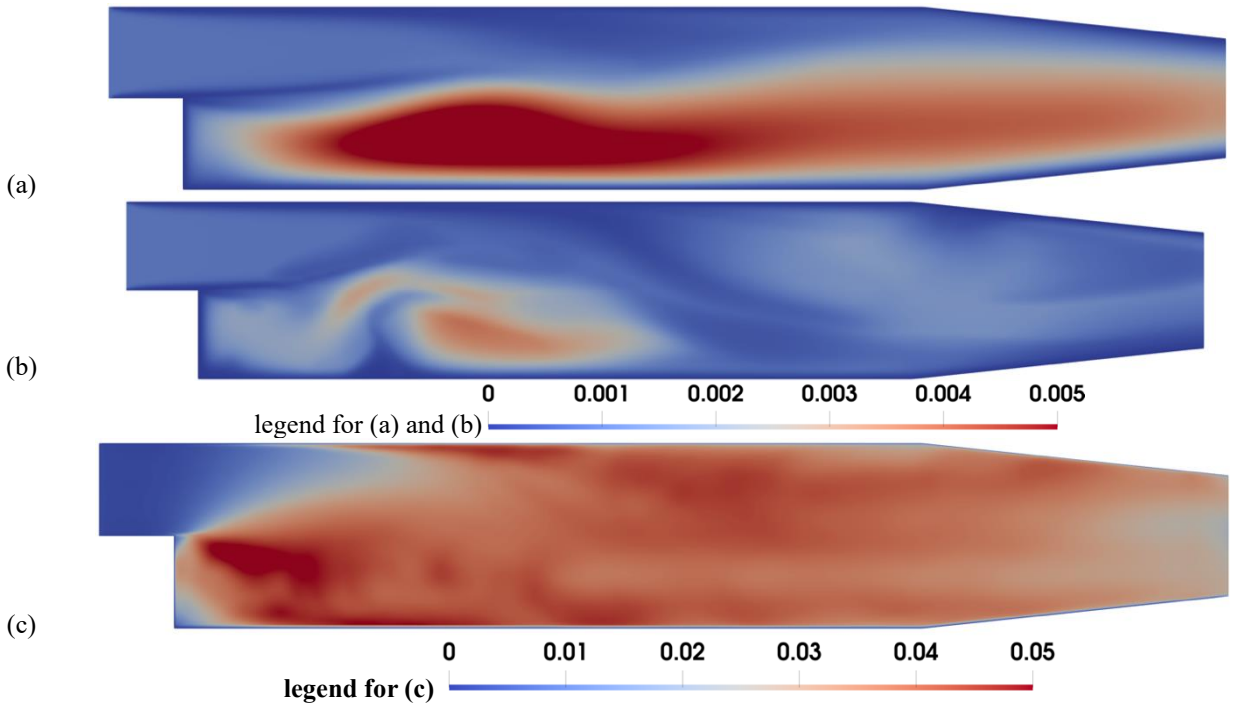

Fig. 11 Comparison of eddy viscosity contours (m^2/s^2) from LES and RANS)simulations for the PitzDaily case: (a) k-ε RANS, (b) k-ω SST RANS, and (c) reference LES data. The RANS models fail to predict the eddy viscosity compared to the LES benchmark accurately. The limitations inherent in eddy viscosity turbulence modeling approaches result in notable disparities between the predicted and observed velocity and pressure fields, as evidenced by the comparative contours in Figures 12 and 13

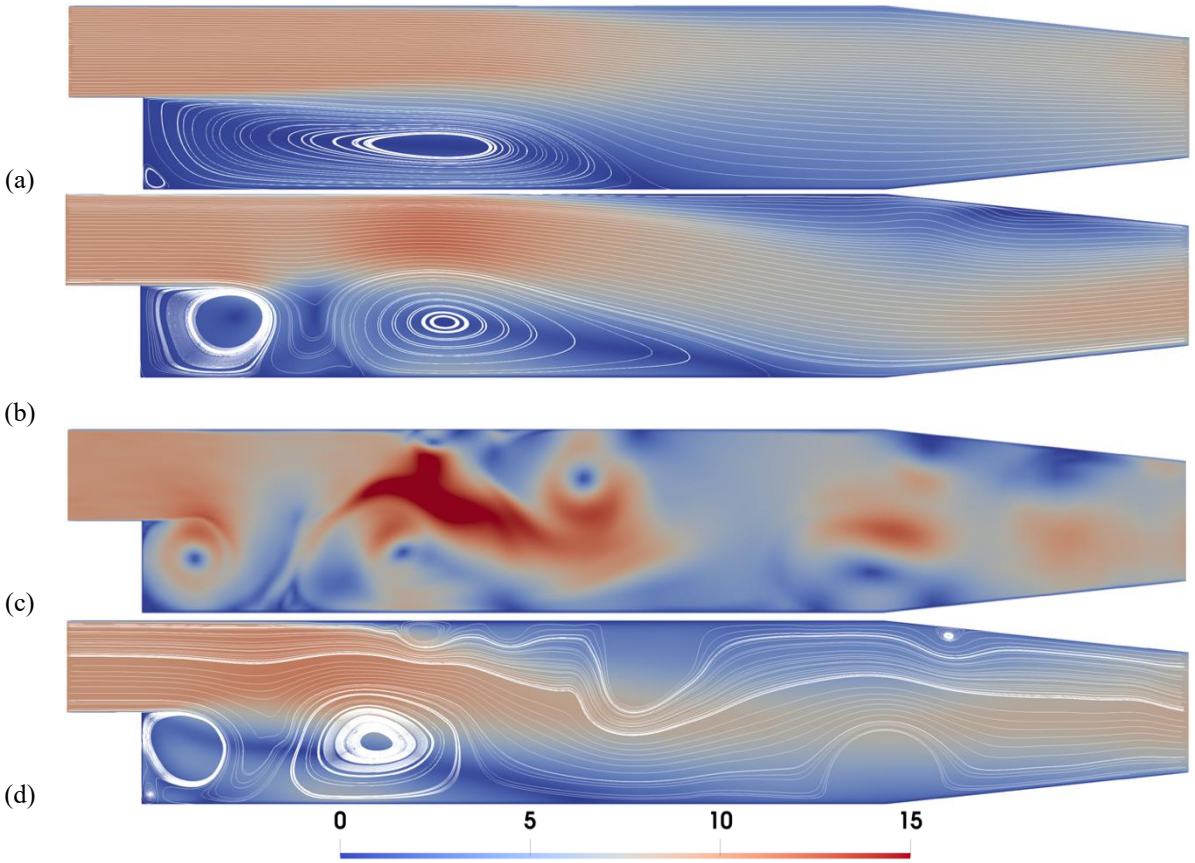

Fig. 12 Comparison of velocity contours (m/s) from LES and RANS simulations for the PitzDaily case: (a) k-ε RANS, (b) k-ω SST RANS, (c) instantaneous LES, and (d) time-averaged LES. The RANS models fail to predict the velocity field accurately compared to the LES benchmark. The instantaneous LES velocity contours exhibit unsteady, turbulent fluctuations, while the time-averaged LES results provide a smoother mean velocity field that can be directly compared to the RANS predictions

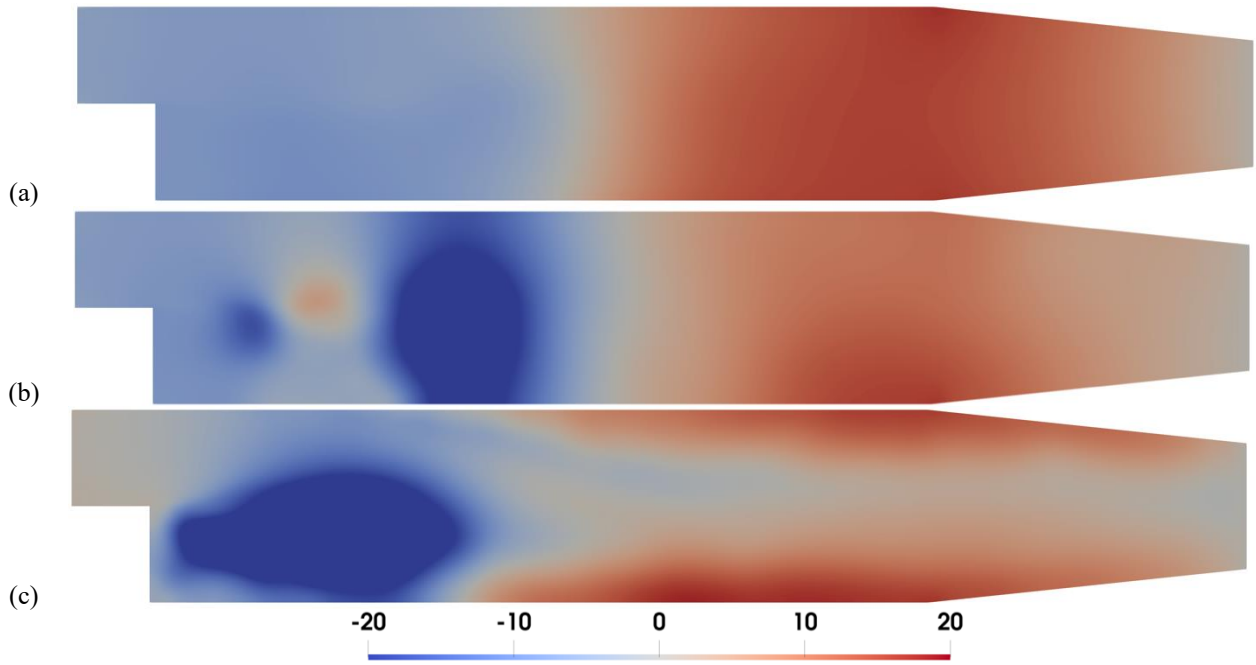

Fig. 13 Comparison of pressure contours (Pa) from Large Eddy Simulation (LES) and Reynolds-Averaged Navier-Stokes (RANS) simulations for the PitzDaily case: (a) k-ε RANS, (b) k-ω SST RANS, and (c) time-averaged LES. The RANS models fail to accurately predict the pressure distribution compared to the LES benchmark, with the k-ε model underpredicting the negative pressures and the k-ω SST model incorrectly predicting the distribution of the negative pressures. These discrepancies are directly linked to the inaccuracies in eddy viscosity modeling by the RANS closures, as shown in Fig. 11. These results further support the conclusion that the eddy viscosity is critical in shaping the flow behavior and pressure distributions around bluff bodies, which is accurately captured by the ML approach but not by the RANS models in this study

Figure 7 comprehensively compares roof pressures from the ML, LES, and RANS simulations. The figure highlights the differences in pressure distributions among the models, with the ML model exhibiting a balance between the two RANS models. This balance is crucial for understanding the aerodynamics of the roof, as it affects the separation bubble and flow reattachment.

The velocity contours in Fig. 8 provide further insight into the flow behavior. The k-ε closure exhibits a short separation bubble with rapid reattachment. In contrast, the k-ω SST closure shows a longer separation bubble that remains open towards the leeward side of the roof. The ML model, on the other hand, shows a separation bubble longer than the k-ε model but with reattachment close to the leeward side of the roof. This variation in flow behavior is closely tied to eddy viscosity, as shown in Fig. 9. The eddy viscosity contours in Fig. 9 reveal that the k-ε closure exhibits higher eddy viscosity, increasing the chances of early flow reattachment.

In contrast, the k-ω SST closure has the lowest eddy viscosity on the entire roof, associated with no flow reattachment. The ML model, which balances the eddy viscosity between the two RANS closures, shows lower eddy viscosity near the windward side but higher near the leeward side, leading to delayed flow reattachment. This variation in eddy viscosity plays a critical role in the flow behavior and pressure distributions observed in the simulations.

The significant differences in eddy viscosity among the models, as observed in Fig. 9, profoundly impact the flow field. The ML model's eddy viscosity distribution, in particular, is distinct from the k-ε and k-ω SST closures, resulting in a unique flow behavior. This observation is consistent with the findings of the PitzDaily problem study, which highlights the sensitivity of flow physics to small changes in eddy viscosity. The velocity contours in Fig. 12 and the pressure distributions in Fig. 13 further support this conclusion, demonstrating that the eddy viscosity is critical in shaping the flow behavior and pressure distributions around the bluff body.

The results of this study underscore the importance of considering eddy viscosity in understanding the aerodynamics of buildings. The ML model balances the eddy viscosity between the two RANS closures and accurately represents flow behavior and pressure distributions. This discovery has significant implications for developing more precise simulation models and a deeper understanding of the complex interactions between flow, pressure, and eddy viscosity.

This paper demonstrates the potential of ML techniques to accelerate numerical solutions, enabling RANS simulations to yield accurate results that would otherwise require high-fidelity, time-consuming simulations like LES. The deep learning approach to accelerating CFD simulations by substituting the turbulence closure with a neural network can provide significant speedups compared to traditional hybrid RANS-LES methods. LES is not a pure LES, as it employs RANS for near-wall treatment. While hybrid RANS-LES methods still require solving the complete set of RANS or

LES equations, the deep learning approach trains a surrogate model to directly predict the turbulent eddy viscosity without needing to solve the full RANS equations, potentially providing order-of-magnitude reductions in computational time. The deep learning framework TensorFlowFoam enables deploying the trained neural network directly within OpenFOAM to accelerate RANS simulations, allowing for end-to-end acceleration (Maulik et al., 2021). Since the training data is obtained from LES, the machine learning-based RANS (ML-RANS) results are close to those from LES. This study demonstrates that CFD simulations with machine learning took approximately 6.27 minutes, compared to 44.3 minutes for simulations using the k-ω SST turbulence closure and 5.6 hours for LES. The ML-RANS approach provided a speedup of more than 50 times while maintaining accuracy comparable to LES in estimating aerodynamic pressures.

Additionally, we emphasize the importance of developing improved turbulence closures to enhance RANS and LES simulations. Accurately modeling eddy viscosity is critical to achieving this goal, which can lead to faster and more accurate simulations of mean pressures. Furthermore, a better understanding of RANS simulations for improved turbulence closures is crucial for more accurate LES simulations, as RANS closures are utilized at the sub-grid scale.

The study highlights the potential of developing new solvers and employing machine learning to enable the rapid investigation of new aeronautical designs to improve performance and achieve efficient and reliable designs. Finally, we suggest that the eddy viscosity may vary with the inflow velocity, and a dimensionless eddy viscosity number could be developed to account for this effect. This approach could treat flows at high Reynolds numbers by adjusting the turbulence and, hence, the eddy viscosity in the shear layer.

In a different application, Sanhueza et al. (2023) proposed a machine-learning approach to improve the predictions of traditional RANS turbulence closures in channel flows with variable thermophysical properties (Sanhueza et al., 2023). The developed machine learning model acts as a nonlinear interpolator for DNS cases, reducing the modeling error on the velocity profile from 23.4% to 4.0%. The study concludes that the proposed methodology is a valid alternative to improve RANS turbulence models in flows with substantial variations in their thermophysical properties without introducing prior modeling assumptions. This finding aligns with the current study, as providing high-quality data for machine learning training can improve the predictions of RANS simulations. Similarly, Liu et al. (2023) proposed a bounded normalization method to improve the extrapolation capability of an iterative machine-learning-based RANS turbulence estimation framework. The improved framework demonstrated accurate prediction capability even when Reynolds numbers are beyond the training range (Liu et al., 2023). The proposed method was tested in channel flows and a spatially developing boundary layer, showing better performance than the conventional normalization method.

Understanding RANS simulations to improve turbulence closures is crucial for achieving faster and more accurate simulations for estimating average pressures. The application of RANS models in sub-grid scale modeling augments the fidelity of LES simulations by improving the accuracy of the resolved scales. Ongoing research in turbulence closures is productive and has the potential to yield models that provide an accurate representation of flow physics, thereby enabling quicker solutions to Navier-Stokes Equations. A key aspect in attaining this goal is precisely predicting the eddy viscosity. It is worth noting that the eddy viscosity varies with inflow velocity, suggesting the development of a dimensionless eddy viscosity number. Adjusting the turbulence and, consequently, the eddy viscosity within the shear layer and wake makes it possible to handle high Reynolds number flows at low Reynolds numbers.

The paper highlights the significance of precise eddy viscosity predictions (magnitude and distribution) for solving RANS equations to forecast roof pressures in wind effects on flat roofs. The results demonstrate that the machine learning-based eddy viscosity modeling approach improves the accuracy of RANS simulations, enabling efficient and dependable design of flat roofs in wind-prone regions. Accurate eddy viscosity prediction in RANS simulations is critical to improve the prediction of roof pressures on flat roofs. These results offer valuable insights for designing and engineering flat roof structures to optimize performance and enhance safety in real-world applications.

5. CONCLUSION

This paper applies deep learning to enhance the precision of RANS simulations for wind-induced pressures on bluff bodies. We refined the eddy viscosity estimation by training a neural network model on LES data for various bluff body geometries, including a flat-roof building and forward/backward facing steps, surpassing the k-ε and k-ω SST turbulence closures. The ML approach closely aligns the new RANS predictions with LES data and experimental results, particularly in the separation zone and shear layer.

The study highlights significant discrepancies in eddy viscosity between the ML-based model and traditional RANS closures. The ML model predicts higher eddy viscosity values near the leeward side of the roof, in the separation zone and wake region. In comparison, traditional RANS closures show lower values in this zone. Conversely, RANS closures exhibit higher eddy viscosity near the upper boundary of the computational domain around a low-rise building. The k-ε closure exhibits higher eddy viscosity near the windward side of the roof, resulting in faster flow reattachment, with extreme negative pressure near the windward side (due to a small tight separation bubble) and much lower negative pressure on the rest of the roof.

Both conventional RANS closures failed to accurately predict the eddy viscosity in the PitzDaily problem compared to the LES reference data. These inaccuracies lead to significant discrepancies in the

velocity and pressure contours, supporting the hypothesis that the failure of RANS simulations to predict roof pressures is due to the inaccurate modeling of eddy viscosity in the separation bubble and shear layer.

A sensitivity analysis on the ML model, manipulating eddy viscosity values, shows that the magnitude and distribution of eddy viscosity govern flow physics in RANS equations. Higher eddy viscosity increases early flow reattachment, while the ML model's balanced viscosity accurately represents flow behavior and pressure distributions. These findings underscore the importance of eddy viscosity in understanding building aerodynamics.

The ML method significantly reduces computational time, converging in 6.27 minutes compared to 5.6 hours for LES, achieving a speedup of over 50 times. The ML approach followed in this study enables direct deployment of the trained neural network within OpenFOAM, further accelerating RANS simulations.

This research reveals the limitations of traditional RANS closures and demonstrates the potential of ML to improve and accelerate numerical simulations of bluff body aerodynamics, as well as a tool for understanding the fundamental physics in fluid mechanics and aerodynamics. Accurate prediction of eddy viscosity in the separation zone and shear layer is crucial, and the proposed ML-based approach significantly reduces computational costs while enhancing accuracy. These advancements can be extended to solving other aerodynamics, fluid mechanics, and environmental problems.

ACKNOWLEDGMENTS

The author received funding from the Louisiana Board of Regents [LEQSF(2022–25)-RD-B-02]. The author also received funding from the LSU Institute for Energy Innovation (Funding Phase 1). The findings are the author's and do not necessarily represent the sponsor's opinion.

CONFLICT OF INTEREST

The author has no conflicts to disclose.

AUTHOR CONTRIBUTIONS

A. M. Aly: Conceptualization, methodology, software, formal analysis, investigation, data curation, writing - original draft, writing - review & editing, visualization.

REFERENCES

Ai, Z. T., & Mak, C. M. (2015). Large-eddy simulation of flow and dispersion around an isolated building: analysis of influencing factors. *Computers and Fluids*, *118*, 89–100. https://doi.org/10.1016/j.compfluid.2015.06.006

Akhlaghi, M., Asadbeigi, M., & Ghafoorian, F. (2023). Novel CFD and DMST dual method parametric study and optimization of a darrieus vertical axis wind turbine. *Journal of Applied Fluid Mechanics*, *17*(1), 205–218. https://doi.org/10.47176/jafm.17.1.1985

Aly, A., & Dougherty, E. (2021). Bridge pier geometry effects on local scour potential: A comparative study. *Ocean Engineering*, https://doi.org/10.1016/j.oceaneng.2021.109326

Aly, A. M. (2014). Atmospheric boundary-layer simulation for the built environment: Past, present and future. *Building and Environment*, *75*, 206–221. https://doi.org/10.1016/j.buildenv.2014.02.004

Aly, A. M. (2016). On the evaluation of wind loads on solar panels: The scale issue. *Solar Energy*, *135*, 423–434. https://doi.org/10.1016/j.solener.2016.06.018

Aly, A. M., & Bitsuamlak, G. (2013). Aerodynamics of ground-mounted solar panels: Test model scale effects. *Journal of Wind Engineering and Industrial Aerodynamics*, *123*, 250–260. https://doi.org/10.1016/j.jweia.2013.07.007

Aly, A. M., & Clarke, J. (2023). Wind design of solar panels for resilient and green communities: CFD with machine learning. *Sustainable Cities and Society*, *94*, 104529. https://doi.org/10.1016/j.scs.2023.104529

Aly, A. M., & Dragomirescu, E. (2018). *Wind engineering for natural hazards: modeling, simulation, and mitigation of windstorm impact on critical infrastructure*. American Society of Civil Engineers. https://doi.org/10.1061/9780784415153

Aly, A. M., & Gol-Zaroudi, H. (2020). Peak pressures on low rise buildings: CFD with LES versus full scale and wind tunnel measurements. *Wind and Structures, An International Journal*, *30*(1), 99–117. https://doi.org/10.12989/was.2020.30.1.099

Aly, A. M., Khaled, M. F., & Clancy, R. (2022). Large-scale open-jet testing: a new frontier in structural wind engineering. *Engineering Structures*, *266*, 114567. https://doi.org/10.1016/j.engstruct.2022.114567

Banari, A., Hertel, D., Schlink, U., Hampel, U., & Lecrivain, G. (2023). Simulation of particle resuspension by wind in an urban system. *Environmental Fluid Mechanics*, *23*(1), 41–63. https://doi.org/10.1007/s10652-022-09905-x

Bao, K., Zhang, X., Peng, W., & Yao, W. (2023). Deep learning method for super-resolution reconstruction of the spatio-temporal flow field. *Advances in Aerodynamics*. https://doi.org/10.1186/s42774-023-00148-y

Chen, S., Qiu, J., Yang, H., Yuan, W., & Gao, Z. (2023). Deep learning for inverse design of low-boom supersonic configurations. *Advances in Aerodynamics*. https://doi.org/10.1186/s42774-023-00145-1

Dickison, M., Ghaleeh, M., Milady, S., Wen, L. T., & Al Qubeissi, M. (2020). Investigation into the aerodynamic performance of a concept sports car. *Journal of Applied Fluid Mechanics*, *13*(2), 583–601.

https://doi.org/10.29252/jafm.13.02.30179

Duraisamy, K., Iaccarino, G., & Xiao, H. (2019). Turbulence modeling in the age of data. In *Annual Review of Fluid Mechanics*. https://doi.org/10.1146/annurev-fluid-010518-040547

ElDegwy, A., Elsayed, A., & Darwish, M. (2022). Aerodynamics of ancient egyptian obelisks and their structural response to boundary layer wind. *Environmental Fluid Mechanics*, *22*(5), 1035–1053. https://doi.org/10.1007/s10652-022-09877-y

Ferreira, A. D., Thiis, T., Freire, N. A., & Ferreira, A. M. C. (2019). A wind tunnel and numerical study on the surface friction distribution on a flat roof with solar panels. *Environmental Fluid Mechanics*, *19*, 601–617. http://dx.doi.org/10.1007%2Fs10652-018-9641-5

Fukami, K., Fukagata, K., & Taira, K. (2019). Super-resolution reconstruction of turbulent flows with machine learning. *Journal of Fluid Mechanics*, *870*, 106–120. https://doi.org/10.1017/jfm.2019.238

Gargallo-Peiró, A., Avila, M., Owen, H., Prieto-Godino, L., & Folch, A. (2018). Mesh generation, sizing and convergence for onshore and offshore wind farm Atmospheric Boundary Layer flow simulation with actuator discs. *Journal of Computational Physics*. https://doi.org/10.1016/j.jcp.2018.08.031

Geneva, N., & Zabaras, N. (2019). Quantifying model form uncertainty in Reynolds-averaged turbulence models with Bayesian deep neural networks. *Journal of Computational Physics*, *383*, 125–147. https://doi.org/10.1016/j.jcp.2019.01.021

Gnatowska, R. (2019). Wind-induced pressure loads on buildings in tandem arrangement in urban environment. *Environmental Fluid Mechanics*, *19*(3), 699–718. https://doi.org/10.1007/s10652-018-9646-0

Guichard, R. (2019). Assessment of an improved Random Flow Generation method to predict unsteady wind pressures on an isolated building using Large-Eddy Simulation. *Journal of Wind Engineering and Industrial Aerodynamics*, *189*, 304–313. https://doi.org/10.1016/j.jweia.2019.04.006

Jones, W. P., & Launder, B. E. (1973). The calculation of low-Reynolds-number phenomena with a two-equation model of turbulence. *International Journal of Heat and Mass Transfer*, *16*(6), 119–1130. https://doi.org/10.1016/0017-9310(73)90125-7

Khaled, M., Aly, A., & Elshaer, A. (2021). Computational efficiency of CFD modeling for building engineering: An empty domain study. *Journal of Building Engineering*. https://doi.org/10.1016/j.jobe.2021.102792

Khaled, M. F., & Aly, A. M. (2022). Assessing aerodynamic loads on low-rise buildings considering Reynolds number and turbulence effects: a review. *Advances in Aerodynamics*, *4*(1), 1–33. https://doi.org/10.1186/s42774-022-00114-0

Khaled, M. F., & Aly, A. M. (2023). Augmenting external surface pressures' predictions on isolated low-rise buildings using CFD simulations. *Wind and Structures, An International Journal*, *37*(4), 255–274. https://doi.org/10.12989/was.2023.37.4.255

Kochkov, D., Smith, J. A., Alieva, A., Wang, Q., Brenner, M. P., & Hoyer, S. (2021). Machine learning–accelerated computational fluid dynamics. *Proceedings of the National Academy of Sciences of the United States of America*. https://doi.org/10.1073/pnas.2101784118

Kundu, P. K., Cohen, I. M., & Dowling, D. R. (2012). *Fluid Mechanics*. Academic Press. https://doi.org/10.1016/B978-0-12-382100-3.10008-3

Le, H., Moin, P., & Kim, J. (1997). Direct numerical simulation of turbulent flow over a backward-facing step. *Journal of Fluid Mechanics*, *330*, 349–374. https://doi.org/https://doi.org/10.1017/S0022112096003941

Li, T., Zhang, J., Rashidi, M. M., & Yu, M. (2019). On the reynolds-averaged navier-stokes modelling of the flow around a simplified train in crosswinds. *Journal of Applied Fluid Mechanics*, *12*(2), 551–563. https://doi.org/10.29252/jafm.12.02.28958

Lim, H. C., Castro, I. P., & Hoxey, R. P. (2007). Bluff bodies in deep turbulent boundary layers: Reynolds-number issues. *Journal of Fluid Mechanics*, *571*, 97–118. https://doi.org/10.1017/S0022112006003223

Liu, L., & Stevens, R. J. A. M. (2020). Wall modeled immersed boundary method for high Reynolds number flow over complex terrain. *Computers and Fluids*. https://doi.org/10.1016/j.compfluid.2020.104604

Liu, W., Fang, J., Rolfo, S., Moulinec, C., & Emerson, D. R. (2021). An iterative machine-learning framework for RANS turbulence modeling. *International Journal of Heat and Fluid Flow*, *90*, 108822. https://doi.org/10.1016/j.ijheatfluidflow.2021.108822

Liu, W., Fang, J., Rolfo, S., Moulinec, C., & Emerson, D. R. (2023). On the improvement of the extrapolation capability of an iterative machine-learning based RANS Framework. *Computers & Fluids*, 105864. https://doi.org/10.1016/j.compfluid.2023.105864

Ma, K., & Lai, H. (2016). Comparison of five two-equation turbulence models for calculation of flow in 90 curved rectangular ducts. *Journal of Applied Fluid Mechanics*, *9*(6), 2917–2931. https://doi.org/10.29252/jafm.09.06.25568

Mahboub, A., Bouzit, M., & Ghenaim, A. (2022). Effects of different shaped cavities and bumps on flow structure and wing performance. *Journal of Applied Fluid Mechanics*, *15*(6), 1649–1660. https://doi.org/10.47176/jafm.15.06.1108

Majchrzak, M., Marciniak-Lukasiak, K., & Lukasiak, P. (2023). A Survey on the application of machine

learning in turbulent flow simulations. *Energies*, *16*(4), 1755. https://doi.org/10.3390/en16041755

Malaspinas, O., & Sagaut, P. (2014). Wall model for large-eddy simulation based on the lattice Boltzmann method. *Journal of Computational Physics*. https://doi.org/10.1016/j.jcp.2014.06.020

Maulik, R., Sharma, H., Patel, S., Lusch, B., & Jennings, E. (2021). *Deploying deep learning in OpenFOAM with TensorFlow*. AIAA Scitech 2021 Forum (p. 1485). https://doi.org/10.2514/6.2021-1485

Menter, F. R. (1992). *Improved two-equation turbulence models for aerodynamic flows. NASA Technical Manual 103975*.

Mitchell, T. M. (1997). *Machine Learning*. McGraw-Hill.

Orszag, S. A. (1970). Analytical theories of turbulence. *Journal of Fluid Mechanics*, *41*(2), 363–386. https://doi.org/10.1017/S0022112070000642

Pathak, J., Mustafa, M., Kashinath, K., Motheau, E., Kurth, T., & Day, M. (2020). Using machine learning to augment coarse-grid computational fluid dynamics simulations. 1–8. https://doi.org/arXiv:2010.00072

Richards, P. J., & Hoxey, R. P. (2002). Unsteady flow on the sides of a 6m cube. *Journal of Wind Engineering and Industrial Aerodynamics*, *90*(12–15), 1855–1866. https://doi.org/10.1016/S0167-6105(02)00293-3

Richards, P. J., & Hoxey, R. P. (2012). Pressures on a cubic building-Part 2: Quasi-steady and other processes. *Journal of Wind Engineering and Industrial Aerodynamics*, *102*, 87–96. https://doi.org/10.1016/j.jweia.2011.11.003

Samuel, A. L. (1959). Some studies in machine learning using the game of checkers. *IBM Journal of Research and Development*, *3*(3), 210–229. https://doi.org/10.1147/rd.33.0210

Samuel, A. L. (1962). Artificial Intelligence: A frontier of automation. *The ANNALS of the American Academy of Political and Social Science*, *340*(1), 10–20. https://doi.org/10.1177/000271626234000103

San, B., Zhao, Y., & Qiu, Y. (2019). Numerical simulation and optimization study of surface pressure and flow field around a triangular prism behind a porous fence. *Environmental Fluid Mechanics*, *19*, 969–987. https://link.springer.com/article/10.1007/s10652-019-09695-9

Sanhueza, R. D., Smit, S. H. H. J., Peeters, J. W. R., & Pecnik, R. (2023). Machine learning for RANS turbulence modeling of variable property flows. *Computers & Fluids*, *255*, 105835. https://doi.org/10.1016/j.compfluid.2023.105835

Sharma, A., Mittal, H., & Gairola, A. (2019). Wind-induced forces and flow field of aerodynamically modified buildings. *Environmental Fluid Mechanics*, *19*, 1599–1623. http://dx.doi.org/10.1007%2Fs10652-019-09687-9

Singh, A. P., Medida, S., & Duraisamy, K. (2017). Machine-learning-augmented predictive modeling of turbulent separated flows over airfoils. *AIAA Journal*. https://doi.org/10.2514/1.J055595

Slotnick, J., Khodadoust, A., Alonso, J., & Darmofal, D. (2014). *CFD vision 2030 study: A path to revolutionary computational aerosciences*. *NNASA/CR-2014-218178*.

Smolarkiewicz, P. K., Sharman, R., Weil, J., Perry, S. G., Heist, D., & Bowker, G. (2007). Building resolving large-eddy simulations and comparison with wind tunnel experiments. *Journal of Computational Physics*. https://doi.org/10.1016/j.jcp.2007.08.005

Thuerey, N., Weissenow, K., Prantl, L., & Hu, X. (2020). Deep learning methods for reynolds-averaged navier-stokes simulations of airfoil flows. *AIAA Journal*, *58*(1), 25–36. https://doi.org/10.48550/arXiv.1810.08217

Ti, Z., Deng, X. W., & Yang, H. (2020). Wake modeling of wind turbines using machine learning. *Applied Energy*. https://doi.org/10.1016/j.apenergy.2019.114025

TienPhuc, D., ZhengQi, G., & Zhen, C. (2015). Numerical simulation of the flow field around generic formula one. *Journal of Applied Fluid Mechanics*, *9*(1), 443–450. https://doi.org/10.18869/acadpub.jafm.68.224.24260

Wadi Al-Fatlawi, A., Hashemi, J., Hossain, S., & El Haj Assad, M. (2024). Applying machine learning in CFD to study the impact of thermal characteristics on the aerodynamic characteristics of an airfoil. *Journal of Applied Fluid Mechanics*, *17*(4), 742–755. https://doi.org/10.47176/jafm.17.4.2276

Xingjun, H., Yufei, L., Keyuan, S., Peng, G., & Jingyu, W. (2023). Suppressing methods of the pressure fluctuation in open jet wind tunnels. *Journal of Applied Fluid Mechanics*, *16*(10), 1901–1915. https://doi.org/10.47176/jafm.16.10.1889

Yan, B. W., & Li, Q. S. (2017). Detached-eddy and large-eddy simulations of wind effects on a high-rise structure. *Computers and Fluids*, *150*, 74–83. https://doi.org/10.1016/j.compfluid.2017.02.009

Zan, B. W., Han, Z. H., Xu, C. Z., Liu, M. Q., & Wang, W. Z. (2022). High-dimensional aerodynamic data modeling using a machine learning method based on a convolutional neural network. *Advances in Aerodynamics*. https://doi.org/10.1186/s42774-022-00128-8

Zhang, J., Gao, G., Liu, T., & Li, Z. (2017). Shape optimization of a kind of earth embankment type windbreak wall along the Lanzhou-Xinjiang railway. *Journal of Applied Fluid Mechanics*, *10*(4), 1189–1200. https://doi.org/10.18869/acadpub.jafm.73.241.27353

Zhang, Z. Q., Liu, H. L., Liu, Z., Zhang, Z., Cheng, G. G., Wang, X. D., & Ding, J. N. (2019). Anisotropic interfacial properties between monolayered black phosphorus and water. *Applied Surface Science*.

https://doi.org/10.1016/j.apsusc.2019.01.037

Zhao, W., Jiang, L., Yao, S., & Chen, W. (2021). Data-driven nonlinear constitutive relations for rarefied flow computations. *Advances in Aerodynamics*. https://doi.org/10.1186/s42774-021-00085-8

Zhao, Y., Akolekar, H. D., Weatheritt, J., Michelassi, V., & Sandberg, R. D. (2020). RANS turbulence model development using CFD-driven machine learning. *Journal of Computational Physics*. https://doi.org/10.1016/j.jcp.2020.109413

Zhou, L. (2017). *Numerical modelling of scour in steady flows* [Université de Lyon]. https://tel.archives-ouvertes.fr/tel-01598600

Zhu, L., Zhang, W., & Tu, G. (2022). Generalization enhancement of artificial neural network for turbulence closure by feature selection. *Advances in Aerodynamics*. https://doi.org/10.1186/s42774-021-00088-5